Effect of Microstructure and Loading Rate on the Fracture Behavior of Titanium–10V–2Fe–3A1

J. H. GIOVANOLA*, R. W. KLOPP*, D. A. SHOCKEY*
and A. T. WERNER**

**Metallurgy and Fracture Mechanics Program, SRI International, Menlo Park, CA 94025, USA*

***Presently with FMC Corp., San Jose, CA 95108, USA*

ABSTRACT

Initiation and propagation toughness of Ti-10V-2Fe-3Al in three microstructural conditions were measured under static and dynamic loads using bend tests. Materials of equivalent strengths, but having 40%, 12% and 0% primary alpha phase, exhibited similar static and dynamic initiation toughnesses but markedly different propagation toughnesses. Fractographic evidence suggests that primary alpha enhances propagation toughness by a resistance curve effect rather than a crack velocity effect.

KEYWORDS

Ti-10V-2Fe-3Al; primary α phase; β phase; dynamic fracture; initiation toughness; propagation toughness; shear lips.

INTRODUCTION

Advances in materials science have improved our ability to control the microstructure of metallic alloys to achieve given mechanical and fracture properties. The process of designing alloys is still to a great degree empirical because the understanding of how component phases and microstructural features contribute to the observed behavior of a material is far from complete. Moreover, the influence of loading parameters such as the loading rate on the material response is not fully established. However, understanding the role of microstructure and loading rate on the fracture behavior of metallic alloys is a key element in attempting to improve properties by microstructural control.

This paper summarizes preliminary results of an investigation to establish how microstructural condition and loading rate influence the fracture behavior of a near-β titanium alloy, Ti-10V-2Fe-3Al. A more extensive account of the investigation will be presented in separate papers in the open literature.

Plates of Ti-10V-2Fe-3Al were heat treated to produce three microstructures with different levels of primary alpha phase (α_p). Tests were then performed on these three microstructures to determine the static and dynamic initiation fracture toughness and the dynamic crack propagation toughness. Fractographic and metallographic examinations were conducted to establish the micromechanisms of failure and explain the observed fracture behavior.

SPECIMEN MATERIALS

We tested specimens machined from 22.6-mm-finished thickness plates rolled from a single ingot of Ti-10V-2Fe-3Al. This alloy has the advantage that it can be heat treated to achieve a range of microstructures (Duerig and Williams, 1984). The thermomechanical treatment given the initial ingot resulted in a β grain size of approximately 50 to 100 μm. Specimens were solution treated and aged according to three different schedules to produce microstructures with approximately 40%, 12% and 0% α_p, while still achieving approximately the same strength level of 1200 to 1300 MPa. Table 1 summarizes the processing schedules for the three microstructures, and Table 2 presents the engineering tensile test data.

Table 1. Heat treatment conditions for three microstructures

Heat treatment steps	0 % α_p	12 % α_p	40 % α_p
Thermomechanical treatment	α-β forged to 50-mm-thick slab, β annealed at 843°C, β rolled to 30-mm-thick plates, α-β finish rolled to 25-mm-thick plates		
Solution treatment	820°C for 1 hr water quenched	790°C for 1 hr water quenched	760°C for 1 hr water quenched
Aging treatment	560°C for 1 hr salt bath	535°C for 2.5 hr salt bath	500°C for 8 hr salt bath

Table 2. Mechanical properties for three microstructures

Property	0% α_p	12% α_p	40% α_p
Yield strength	1119 MPa	1257 MPa	1123 MPa
Ultimate strength	1186 MPa	1327 MPa	1190 MPa
% Elongation	7.6	6.8	8.4

EXPERIMENTAL PROCEDURES

Dynamic initiation and crack propagation toughnesses were measured using the so-called one-point-bend test (1PBT). The 1PBT produces a smoothly varying stress intensity history and hence an unambiguous measure of dynamic fracture toughness. This experimental technique, briefly reviewed here, is described in detail in Giovanola (1985a). The 1PBT uses a single-edge-cracked specimen and the same testing arrangement as a conventional three-point bend impact test, except that the end supports are removed. When the hammer strikes the center portion of the specimen, that region is accelerated away from the hammer, whereas the end portions of the specimen lag behind because of inertia. The inertial lag causes the specimen to bend and to load the crack tip. The maximum stress intensity amplitude and the duration of the loading are readily adjusted by changing the impact velocity and the specimen geometry, respectively. For materials with low mass densities, the maximum achievable stress intensity amplitude can be increased by adding ballast plates at each end of the specimen to increase inertia (Giovanola, 1985a). We used this technique for the crack propagation experiments performed in this investigation.

The stress intensity history up to the point of crack initiation is obtained by measuring the crack tip strain intensification with a calibrated strain gage placed near the crack tip. The measured strain is then related to the applied stress intensity using a calibration factor, determined experimentally or analytically. A different technique such as photoelasticity, caustics or numerical simulations of the experiments, must be used to obtain the stress intensity factor during crack propagation. We chose the numerical simulation approach for this investigation. Since the simulations were still being performed at the time this paper was written, the results will not be presented here. Rather we will evaluate the dynamic crack propagation behavior on the basis of additional observations.

During the dynamic initiation experiments, we measured the impact force with strain gages mounted on the hammer, the impact velocity and the strain near the initial crack tip. During the crack propagation experiments, we measured the crack propagation history by taking high-speed photographs of the ligament region of the specimen. Further, we measured strains normal to the crack plane at three locations spaced 10 mm apart along the crack path. These strain records provided independent verification of the crack propagation histories and coarse estimates of the stress intensity factor during crack extension.

In the crack propagation tests, we varied the crack speed by varying the impact velocity between 10 and 14 m/s and by varying the initial notch root acuity from a sharp fatigue crack to a 0.40 mm radius.

Standard ASTM E399 three-point-bend fracture tests were performed on all three microstructures to determine the quasi-static initiation toughness.

RESULTS OF FRACTURE EXPERIMENTS

Figure 1 summarizes the results of the crack initiation experiments. Although the data are statistically sparse and the scatter is large, clear trends can be deduced from the initiation results. For each of the microstructures, the initiation toughness increases by a small but discernible amount with increasing loading rate, and the rate sensitivity appears to depend on the microstructure. For microstructures with 40%, 12% and 0% α_p, the average value of the initiation toughness increases by about 18%, 14% and 9%, respectively, when the loading rate is increased from 0.2 to 10^6 MPa$\sqrt{m}$/s. At a given loading rate, the microstructural condition also affects the initiation toughness in a discernible way. Whereas the two microstructures containing primary alpha have approximately the same initiation toughness, the initiation toughness of the material with no primary alpha is 10% to 20% lower.

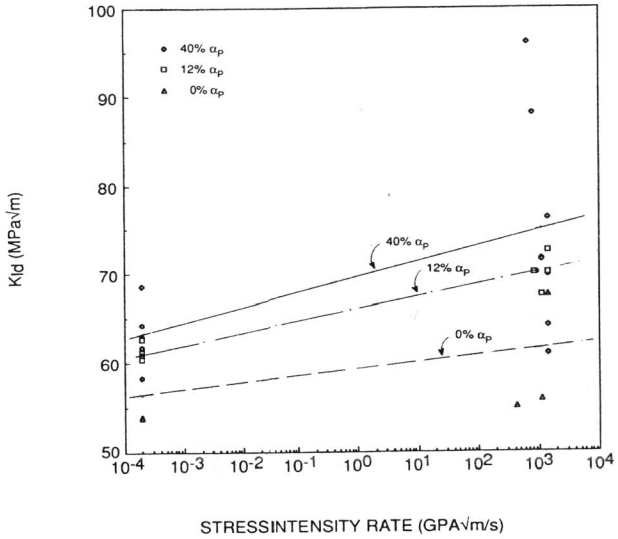

Fig. 1. Summary of crack initiation test results.

In the crack propagation experiments, crack speeds between 50 and 400 m/s were achieved. Crack extension histories measured photographically were in good agreement with histories derived from strain gage data. Figure 2 shows crack extension histories for the three microstructures for identical test conditions and in particular for identical impact velocities and identical stress intensity amplitudes, K_{init}, at the onset of crack extension. The data in Figure 2 indicate that microstructural condition significantly influences the crack propagation behavior, with the overall crack velocity increasing as the α_p decreases. This observation suggests that

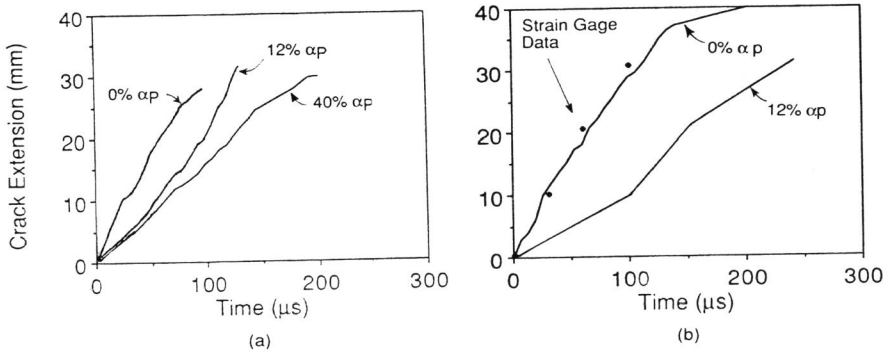

Fig. 2. Crack extension history for specimens tested under identical conditions. V_{imp}= 14 m/s and (a) K_{init} = 95 MPa√m and (b) K_{init} = 70 MPa√m,

the propagation toughness decreases with decreasing α_p content. Three additional observations further support this conclusion.

First, we analyzed the strain records obtained during the crack propagation experiments from the strain gages mounted along the crack path to estimate the dynamic propagation toughness. An approximate analysis based on the solution for a crack moving at constant speed through an infinite plate (Broberg, 1960) was used to relate strain measurements and stress intensity factor. For the range of velocity we investigated (50 to 400 m/s), 40%, 12% and 0% α_p microstructures have an estimated propagation toughness of 190 MPa√m, 160 MPa√m and 90 MPa√m, respectively. Although these toughness values can only be regarded as coarse estimates, they clearly indicate a significant influence of the α_p content. Moreover, the dynamic propagation toughness values appear significantly larger than the initiation toughness value, which is generally not observed at the relatively low crack velocities investigated here.

Second, we measured markedly different shear lip heights on fracture surfaces of specimens with different α_p contents, namely 3.3 mm, 2.4 mm and 1.1 mm for 40%, 12% and 0% α_p, respectively (Fig. 3). These size differences suggest differences in toughness, since the shear lip height is a measure of the plastic zone size, which itself depends on the square of the propagation toughness. Estimates of the plastic zone size at the specimen surface (plane stress) based on the toughnesses derived from the strain gage measurements result in values of 4 mm, 2.4 mm and 0.9 mm for 40%, 12% and 0% α_p, respectively, which are consistent with the observed shear lip values.

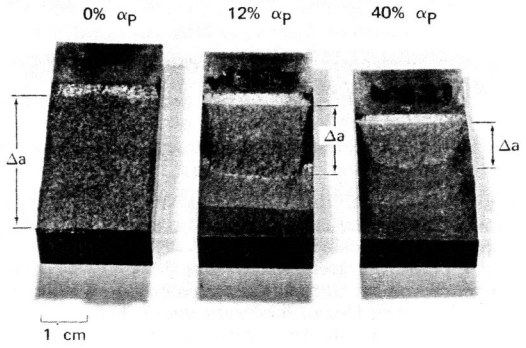

Fig. 3. Fracture surfaces of three microstructures tested under identical conditions.

Figure 3 also illustrates the third observation that demonstrates propagation toughness differences among the three microstructures. Figure 3 shows the fracture surface of fatigue precracked specimens with 40%, 12% and 0% α_p of identical geometry and impacted under identical conditions. The crack extended 12 mm and 20 mm in the 40% and 12% α_p specimens, respectively, whereas it propagated completely through the specimen with 0% α_p. The difference in arrest crack length demonstrates that the three microstructures have different propagation toughnesses. Multiple experiments for the 40% α_p microstructure showed repeatability of the arrest crack length to within 1 mm.

FRACTOGRAPHIC AND METALLOGRAPHIC RESULTS

Figure 4 shows scanning electron microscope (SEM) fractographs taken near the initial fatigue crack front of impact loaded specimens with 40% and 0% α_p. At first inspection, these two surfaces appear to have quite different morphologies, with the 0% α_p specimen displaying smooth grain facets, whereas the 40% α_p specimen appears more textured. However, we also

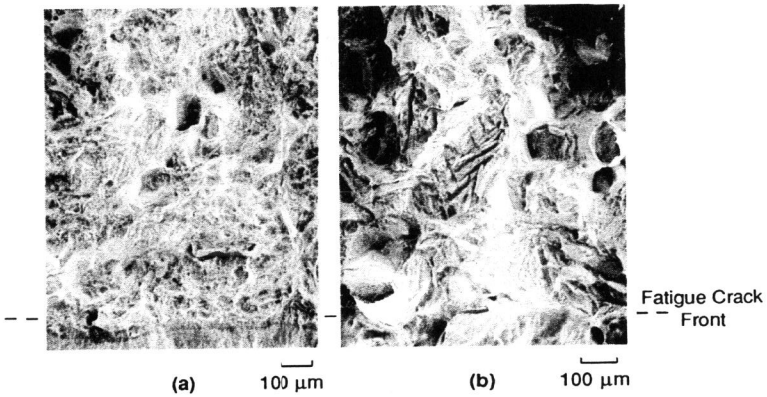

Fig. 4. Scanning electron micrograph of dynamic fracture specimen with (a) 40% α_p and (b) 0% α_p.

observed several similarities. For all three microstructures, we identify two size scales of the fracture surface features. The larger size scale is on the order of many tens of micrometers. Fractographic features of this size scale include grains or grain fragments, cracks perpendicular to the main crack plane, and large stretch and slip regions. The smaller size scale is on the order of many micrometers. Fractographic features of this size consist predominantly of microvoids and often cover the surface of the larger size scale features. The morphology, size and density of the microvoids vary with the microstructural condition and with the loading rate. SEM observations reveal large localized slip and stretch deformations within grains for all three microstructures but particularly for the α_p-containing microstructures. The loading rate also effects some changes in the fracture appearance. The smooth furrows visible in Figure 4(b) at the center of the fracture surface of a dynamically loaded specimen with 0% α_p are not found on statically loaded specimens.

Metallographic cross sections normal to the crack plane reveal collateral damage and the microfracture initiation sites. For all three α_p contents, we observed several 20- to 100-µm deep secondary cracks normal to the main crack plane, as well as isolated microvoids below the main crack plane. In the α_p-containing microstructures, microvoids nucleate preferentially at α_p particles and cracks tend to follow grain boundaries or rows of α_p particles, although we also observed transgranular cracks. For the microstructure with no α_p, voids nucleate

predominantly at grain boundaries and microcracks are to a large extent intergranular. However, we also observed some instances of void nucleation within grains and of transgranular cracks.

Overall, metallographic observations suggest that grain boundary separation by microvoid nucleation and growth may play a key role in controlling the fracture toughness of all three investigated microstructures.

DISCUSSION AND CONCLUSIONS

The present investigation demonstrates that loading rate and α_p content have a relatively small influence on the initiation fracture toughness of Ti-10V-2Fe-3Al, aged to about 1200 MPa strength level. At a given loading rate, decreases from 40% to 0% α_p are accompanied by decreases in initiation toughness of no more than 20%. Changes in loading rate from 0.2 to 10^6 MPa$\sqrt{m}$/s induce increases in toughness of no more than 20%. On the other hand, the α_p content has a pronounced influence on the dynamic crack propagation behavior in the three microstructures studied. For the same impact and crack initiation conditions, the crack speed decreases and the crack is more easily arrested as the α_p content increases. Toughness estimates, which are consistent with observed shear lip sizes, indicate that the propagation toughness at crack speeds between 50 and 400 m/s doubled when the α_p content increased from 0% to 40%.

That the loading rate has only a small influence on the initiation toughness is somewhat surprising in view of the results of Bryant and Wilsdorf (1988). These workers found almost a doubling of the initiation toughness with an increase in loading rate from 1.5 MPa$\sqrt{m}$/s to 13 x 10^3 MPa$\sqrt{m}$/s. However, this difference in loading rate sensitivity, compared with our findings, may be due to the differences in heat treatment, which produces a much lower static fracture toughness in the material investigated by Bryant and Wilsdorf (35.5 MPa$\sqrt{m}$).
The moderate sensitivity of the initiation toughness to the α_p content is also somewhat unexpected. The fractographic and metallographic observations suggest a possible explanation for this behavior. For all three microstructures, grain boundary separation through nucleation and growth of microvoids appears to be an important microfailure mechanism. Therefore, the fracture toughness may be to a large extent controlled by the nature and morphology of the grain boundary phase, by the interface strength and by the mechanisms of grain boundary void nucleation. Since the grain boundary phase is always α, independent of the α_p content, and since the grain strength is approximately the same, it seems reasonable that the initiation toughness is similar in all three microstructures. However, because failure mechanisms other than grain boundary separation were also observed, particularly in the microstructures containing α_p, the proposed explanation for the relative insensitivity of the initiation toughness to α_p content must be substantiated by additional observations.

With respect to the dynamic propagation toughness, two observations warrant discussion: (1) the marked influence of the α_p content on the propagation toughness, despite the limited influence of the α_p content on the initiation toughness and (2) the presumably much higher values of the dynamic propagation toughness compared with the initiation toughness, particularly in the microstructures with 40% and 12% α_p. We believe that the difference in shear lip size plays an important role in promoting both these behaviors. The small differences in initiation toughness and yield stress are sufficient to promote the formation of shear lips of slightly different size, depending on the α_p content. As the crack extends, shear lips act as trailing tensile ligaments; they force the crack front to gradually bow, and they effectively raise the apparent fracture toughness. In turn, the higher apparent toughness promotes larger shear lips. This coupled mechanism is most pronounced in the 40% α_p, which has the largest

estimated initial plastic zone, and least pronounced in the 0% α_p microstructure, which has the smallest estimated initial plastic zone. This postulated mechanism implies that shear lips are simultaneously the cause and evidence of the differences in propagation toughnesses. The postulated mechanism also implies that the elevation in propagation toughness above the initiation toughness is not due to a crack velocity effect, as is often the case in dynamic fracture, but to a resistance curve effect: the propagation toughness increases as a function of crack extension in a manner analogous to the increase observed in static elasto-plastic fracture testing. The dynamic resistance curve concept was invoked earlier to explain similar dynamic fracture observations in high-strength steel (Giovanola, 1985b).

In the next months we will seek more reliable estimates of the propagation toughness values by performing finite element simulations of the experiments. We will continue the fractographic and metallographic observations to elucidate the mechanisms of void nucleation and growth in the microstructures with three α_p contents. We expect these additional data to provide a better and more quantitative understanding of the micromechanisms of fracture in Ti-10V-2Fe-3Al and of the influence of the loading rate and the α_p content on the initiation and propagation toughness.

ACKNOWLEDGMENTS

The work presented in this paper was funded by the Air Force Office of Scientific Research under Contract AFOSR/F49620-86-K-0010DEF, Dr. A. H. Rosenstein, Technical Monitor. The authors would like to thank Dr. T. W. Duerig, Raychem Corp., for advice and numerous helpful discussions on the metallurgy of Ti-10V-2Fe-3Al.

REFERENCES

Broberg, K. B. (1960). The propagation of a brittle crack. *Arkiv Fyhsik*, 18, 159.

Bryant J. D. and H. G. F. Wilsdorf (1988). In: *Impact Loading and Dynamic Behavior of Materials* (C. Y. Chiem, H. D. Kunze and L. W. Meyer, eds.), Vol. I, pp. 145-152, DGM Informationsgesellshaft mbH, Oberursel, West Germany.

Duerig, T. W. and J. C. Williams (1984). In: *Beta Titanium Alloys in the 1980s* (R. R. Boyer and H. W. Rosenberg, eds.), pp. 19-67. The Metallurgical Society of AIME, Warrendale, PA.

Giovanola, J. H. (1985a). In: *ASM Metals Handbook, 9th edition, Vol. 8, Mechanical Testing*, pp. 271-276, American Society for Metals, Metals Park, OH.

Giovanola, J. H. (1985b). In: *Dymat 85, International Conference on Mechanical Behavior of Materials under Dynamic Loading*, pp. C5 171-C5 178, Les Editions de Physique, Les Ulis, France.